Structural characterization of cell-wall polysaccharides purified from chayote (*Sechium edule*) fruit

Jingxuan Ke [a,c,*], Yuhao Zhang [a], Xin Wang [b], Jing Sun [a], Siqi Wang [a], Yanli Ma [a], Qing Guo [c], Zhiqing Zhang [c,*]

[a] *School of Zhang Zhongjing Health Care and Food, Nanyang Institute of Technology, Nanyang 473004, China*
[b] *College of Food Science and Technology, Hebei Agricultural University, Baoding 071000, China*
[c] *College of Food Science, Sichuan Agricultural University, Ya'an 625014, China*

ARTICLE INFO

ABSTRACT

Chayote (*Sechium edule*), an underutilized cucurbit vegetable crop, has gained attention as it exhibits health-promoting properties. However, the primary structure of chayote cell-wall polysaccharides has not been comprehensively studied. In this study, two cell-wall polysaccharides, CP-1 (41.1 KDa) and CP-2 (15.6 KDa), were extracted from chayote, and the structural analysis of CP-1 and CP-2 was carried out by monosaccharide composition analysis, Fourier transform infrared spectroscopy (FTIR), methylation analysis, and nuclear magnetic resonance spectroscopy (NMR). The results demonstrated that CP-1 was a galactan, and CP-2 was an anionic heteropolysaccharide composed of galacturonic acid, galactose, arabinose, rhamnose, glucose, glucuronic acid, mannose, and xylose in the molar ratio of 31.2:26.3:24.9:7.4:6.5:1.9:1.3:0.5. CP-2 has a backbone of → 4)-β-D-Gal*p*-(1 → 3,6)-β-D-Gal*p*-(1 → 3)-β-D-Gal*p*-(1 → 4)-α-D-Gal*p*A-(1→, with branches at O-6 of → 3,6)-β-D-Gal*p*-(1→, consisting of α-L-Ara*f*-(1 → 5)-α-L-Ara*f*-(1 → 4)-β-D-Glc*p*-(1 →. Analysis of the structural and physicochemical properties confirmed the excellent application characteristics of CP-1 and CP-2. Hence, cell-wall polysaccharides of chayote could be used as new polysaccharides materials.

1. Introduction

The plant cell wall is rich in polysaccharides such as cellulose and pectin (Zhao, Moates, Wellner, Collins, Coleman, & Waldron, 2014). Analysis of literature reports suggests that plant polysaccharides exhibit biological activity with moderate or no toxic effects (Wang, Hu, Wang, Yang, Kuang, 2023; Fernandes & Coimbra, 2023). These pieces of evidence support the importance of fruit or vegetable polysaccharides for human health (Ji et al., 2023). Therefore, the research on plant polysaccharides is a hot topic, encompassing extraction methods, structure identification, and more.

Sechium edule, commonly known as chayote, belongs to the gourd family (Cucurbitaceae, subtribe Sicyinae) and is cultivated worldwide as an edible plant (Aung, Ball, & Kushad, 1990). It is characterized by its vigorous vitality and strong adaptability, earning it the reputation of being a "pollution-free" vegetable (Aung, Ball, & Kushad, 1990). The chayote root is an excellent source of starch, while its fruit is rich in non-starch polysaccharides (Castro-Alves & do Nascimento, 2016). Plant

polysaccharides are widely used in food and health products due to their excellent water-holding, thickening, and biological properties. However, the incomplete study on the primary structure of chayote polysaccharide has limited its applications in food, medicine, and other industries. Chayote can be used as a valuable source of polysaccharides in the food and pharmaceutical sectors to expand its potential applications (Vieira, Pinho, Ferreira, & Delerue-Matos, 2019).

Castro-Alves and Nascimento (2016) conducted a study on the biological activity of chayote polysaccharides, which revealed their potential to modulate macrophage function in RAW 264.7 murine macrophages. The biological activity of polysaccharides is influenced by various factors, including molecular weight, monosaccharide composition, linkage, and other structural characteristics (Zhang, Guo, Yan, Feng, & Wan, 2020). Additionally, the water-holding capacity and solubility of cell-wall polysaccharides contribute to their beneficial activities. Gaining a comprehensive understanding of the primary structural characteristics of chayote polysaccharides is essential for studying their potential applications in food and health products. Therefore, a

---

* Corresponding authors.
 E-mail addresses: jingxKe@163.com (J. Ke), zqzhang721@163.com (Z. Zhang).

thorough analysis of the primary structure of polysaccharides is necessary.

However, research on glycoside bonds and the primary structure of cell-wall polysaccharides from chayote is still in its early stages. Researchers are focusing on the total sugar content, molecular weight, and monosaccharide composition (Shiga, Peroni-Okita, Carpita, Lajolo, & Cordenunsi, 2015). Recent studies have indicated that chayote is a valuable source of galactans and arabinan-rich polysaccharides (Shiga, Peroni-Okita, Carpita, Lajolo, & Cordenunsi, 2015). Thus, it can be speculated that the cell-wall polysaccharides of chayote are abundant in galactans and arabinan. The objective of this study is to fractionate the cell-wall polysaccharides of chayote and investigate the structural and main physicochemical properties of its two subfractions (CP-1 and CP-2). Additionally, the study aims to analyze the monosaccharide composition, molecular weight, glycoside bonds, primary structure prediction, and micromorphology of CP-1 and CP-2. This research will establish a structural foundation for further studies on the biological activity of chayote polysaccharides in the context of nutritional science.

2. Materials and methods

2.1. Material and reagents

Green chayote fruits were obtained from the local farmers' market (Ya'an, China) and identified by Prof. Chunbang Ding of the College of Life Science of Sichuan Agricultural University. Chayote fruits were washed thoroughly, cut into pieces, and dried at 60 °C in an air circulation oven for 12 h (Beijing Yongming Medical Instrument Co., Ltd, Beijing, China). The dried chayote pieces (dimensions: approximately 15 cm × 2.5 cm) were milled and passed through an 80-mesh sieve. The chayote powder was mixed with deionized water (1:30 w/v) and hydrolyzed using α-amylase (0.05 g, enzyme activity was 4000 μ/g) at pH 6.0. The experiments were conducted at 60 °C over 30 min (Yang, Mu, & Ma, 2018). The obtained precipitate was washed with deionized water thrice to remove soluble sugar. The final residue was dried at 60 °C in a convective oven under conditions of air circulation. The products were finally milled and passed through an 80-mesh sieve. L-rhamnose, L-fucose, L-arabinose, D-xylose, D-mannose, D-glucose, D-galactose, galacturonic acid, and glucuronic acid were purchased from Sigma–Aldrich (USA). Other reagents were of analytical grade.

2.2. Extraction of crude cell-wall polysaccharides

Chayote cell-wall polysaccharide was extracted according to the method reported in our previous study (Ke, Jiang, Shen, Wu, Liu, & Zhang, 2020). Powdered chayote samples were extracted with water (pH 2) at a liquid/solid ratio of 50:1 (mL/g). The mixture was then submerged in an ultrasonic device for ultrasonic treatment (power: 180 W; time: 40 min; temperature: 70 °C). The supernatant was collected using a Buchner funnel after extraction. The polysaccharides were precipitated by adding two volumes of anhydrous alcohol and stored at 4 °C overnight. The sediment polysaccharides were collected by centrifugation (2700 g, 10 min). Later, the polysaccharides were washed thrice with 95% ethanol. Finally, it was dried at 50 °C and milled to obtain cell-wall polysaccharides.

2.3. Purification of polysaccharides

The polysaccharides have been purified following the method reported by Hong & Ying (2019). The crude polysaccharide solution was loaded on a DEAE-52 column (2.5 × 40 cm) and eluted with deionized water, 0.2 mol·L^{-1} of NaCl, 0.5 mol·L^{-1} of NaCl, and 2.0 mol·L^{-1} of NaCl in sequence, and the volume of each solvent system used during elution was three times the column volume. The fractions were collected, concentrated, dialyzed, and freeze-dried. The fractions were named P-1, P-2, P-3, and P-4.

The prefractionation polysaccharide sample (P-1 and P-2) solutions were loaded on a column (1.5 × 100 cm) loaded with Sephadex-200. The column was connected to a differential detector (RI-502 SHO-DEX), and the sample was eluted with deionized water. Symmetrical peaks appeared in the profiles recorded for the samples. The collected solutions were concentrated using a rotary evaporator and freeze-dried to obtain the purified polysaccharides. The solutions were labeled CP-1 and CP-2.

2.4. Structure analysis

2.4.1. Molecular weight analysis

The weight-average molecular weight (M_w), number-average molecular weight (M_n), and polydispersity (M_w/M_n) values corresponding to CP-1 and CP-2 were recorded using the high-performance gel permeation chromatography (HPGPC) technique. The method previously reported by us was followed to obtain the results (Ke, Jiang, Shen, Wu, Liu, & Zhang, 2020). The calibration equations (lgM_w = -0.2006x + 12.618, R^2 = 0.9960; lgM_n = -0.1805x + 11.673, R^2 = 0.9970) were built using dextran as the standard.

2.4.2. Monosaccharide composition

The compositional monosaccharides (CP-1 and CP-2) were analyzed using the ion chromatography technique following the method outlined in the report by Yang et al. (2018). The reported method was slightly modified to conduct the studies. In summary, the sample was hydrolyzed using trifluoroacetic acid (TFA). The hydrolyzed sample was subjected to analysis using an ICS-5000 system (Thermo Fisher Scientific, USA) equipped with a DionexCarbopacTMPA20 column (3 mm × 150 mm). The eluent consisted of three components: A: H$_2$O, B: 250 mmol·L^{-1} of NaOH, and C: 50 mmol·L^{-1} of NaOH and 500 mmol·L^{-1} of NaOAc. The flow rate was set at 0.3 mL/min, the column temperature was maintained at 30 °C, and the injection volume was 5 μL.

2.4.3. Analysis of spectral profiles

The UV–visible spectral profiles of the purified polysaccharide fractions (CP-1 and CP-2) at a concentration of 1 mg/mL were recorded using a UV–visible spectrophotometer (UV-1600PC, Mapada Instruments, Shanghai, China) in the wavelength range of 200–400 nm (Gao et al., 2020). The Fourier-transform infrared (FTIR) spectra of the purified polysaccharide fractions (CP-1 and CP-2) were obtained using an FTIR instrument (Nicolet iS10, Thermo Fisher Scientific, USA). The spectra were collected following the KBr pellet method (Ke, Jiang, Shen, Wu, Liu, & Zhang, 2020). The samples were scanned in the range of 4000–400 cm^{-1}. The resolution was set to 4 cm^{-1}, and the spectra were acquired by performing 32 scans.

2.4.4. Uronic acid reduction

The reduction of uronic acids in the anionic heteropolysaccharide (CP-2) sample was repeated thrice following the method reported by Chen, Zhu, Ma, Zhang, & Wu (2019).

2.4.5. Methylation analysis

The glycosidic bonds of purified polysaccharides (CP-1 and CP-2) were analyzed following the method reported by Chen et al. (2019). The reported method was slightly modified to conduct the experiments. The samples (2 mg) were mixed with dimethyl sulphoxide (1 mL) and NaOH powder. Subsequently, the mixture was dissolved under the conditions of ultrasonic treatment. Later, 1 mL of methyl iodide was added to the system, and the reaction was continued for 60 min under conditions of magnetic stirring at 30 °C in a water bath. In the end, 2 mL of deionized water was added to the mixture to arrest methylation. The methylated sample was hydrolyzed with TFA (2 mol·L^{-1}) for 90 min and reduced with NaBH$_4$ (60 mg) over 8 h. The mixture was then neutralized using glacial acetic acid, and the solvent was removed. The residue was acetylated using acetic anhydride. The acetylated sample was extracted

four times with dichloromethane. Finally, partially methylated alditol acetates (PMAAs) were analyzed using a Gas Chromatography-Mass Spectrometer system. The samples were analyzed using an RXI-5 SIL MS column under conditions of programmed temperature increase (from 120 to 250 °C) at the rate of 3 °C/min. A steady temperature (250 °C) was maintained for 5 min. The injection and detector temperatures were 250 °C, the carrier gas was helium, and the flow rate was 1 mL/min.

2.4.6. NMR analysis

The purified polysaccharide fractions (CP-1 and CP-2, 50 mg) were dissolved in 0.5 mL of D_2O (99.9 atom%). Following this, the samples were lyophilized, and the process was repeated thrice. The samples were then dissolved in 0.5 mL of D_2O. One-dimensional (1D) and two-dimensional (2D) NMR spectra were recorded at 25 °C on a Bruker Ascend 600 MHz NMR spectrometer with acetone as the internal standard (Chen, Zhu, Ma, Zhang, & Wu, 2019).

2.5. Morphology and ultrastructure analysis

2.5.1. Scanning electron microscope (SEM) analysis

Samples (CP-1 and CP-2) extracted from chayote were subjected to freeze-drying treatment. The morphology of the solid molecules of two purified cell-wall polysaccharide (CP-1 and CP-2) samples was observed using a SEM (SU8020, Hitachi, Japan). Samples were placed on a conductive adhesive plate and sputter coated with gold. The acceleration voltage was 3 kV, and the corresponding magnification rate was 200× (Zhang, Kong, Hao, Zhang, & Zhu, 2020).

2.5.2. Atomic force microscopy (AFM) analysis

The samples (CP-1 and CP-2) were diluted to approximately 10 µg/

mL, and 5 µL of the sample solution was dropped onto a freshly cleaved mica. Following this, the samples were dried in air at room temperature (25 °C). The ultrastructure of CP-1 and CP-2 was observed using the AFM (Dimension Icon, Bruker, Germany) technique at a resolution of 256 × 256 lines and a scanning rate of 1.0 Hz (Qin, Liu, Lv, & Wang, 2020).

2.5.3. X-ray diffraction (XRD) analysis

The crystalline structures of the purified polysaccharides (CP-1 and CP-2) were analyzed using an X-ray Diffractometer (BRUCKER D8 ADVANCE, Bruker, Germany) to obtain their crystal arrangement. The sample was placed flat on the groove of the sample plate and flattened with a glass plate prior to conducting the experiments. The scanning range (2θ angle) was 5–80° (Zhang, Kong, Hao, Zhang, & Zhu, 2020).

3. Results and discussion

3.1. Purification of CP-1 and CP-2

The chayote cell-wall polysaccharide sample was fractionated using a DEAE-52 cellulose column. Fig. 1A presents details of the four fractions named P-1 (9.2%), P-2 (12.6%), P-3 (3.6%), and P-4 (0.5%). The maximum absorbance was recorded when the first fraction (P-1) was eluted using deionized water (Fig. 1A; second yield; 9.2%). This can be potentially attributed to the disappearance of the free monosaccharides from the crude polysaccharide during dialysis. P-1 and P-2 were obtained in higher yields compared to the other two eluted fractions (P-3 and P-4). Therefore, P-1 and P-2 were concentrated, dialyzed, and lyophilized for further study.

The gel permeation chromatography technique was used to purify P-1 and P-2 to obtain the final fractions, i.e., purified CP-1 and CP-2. The
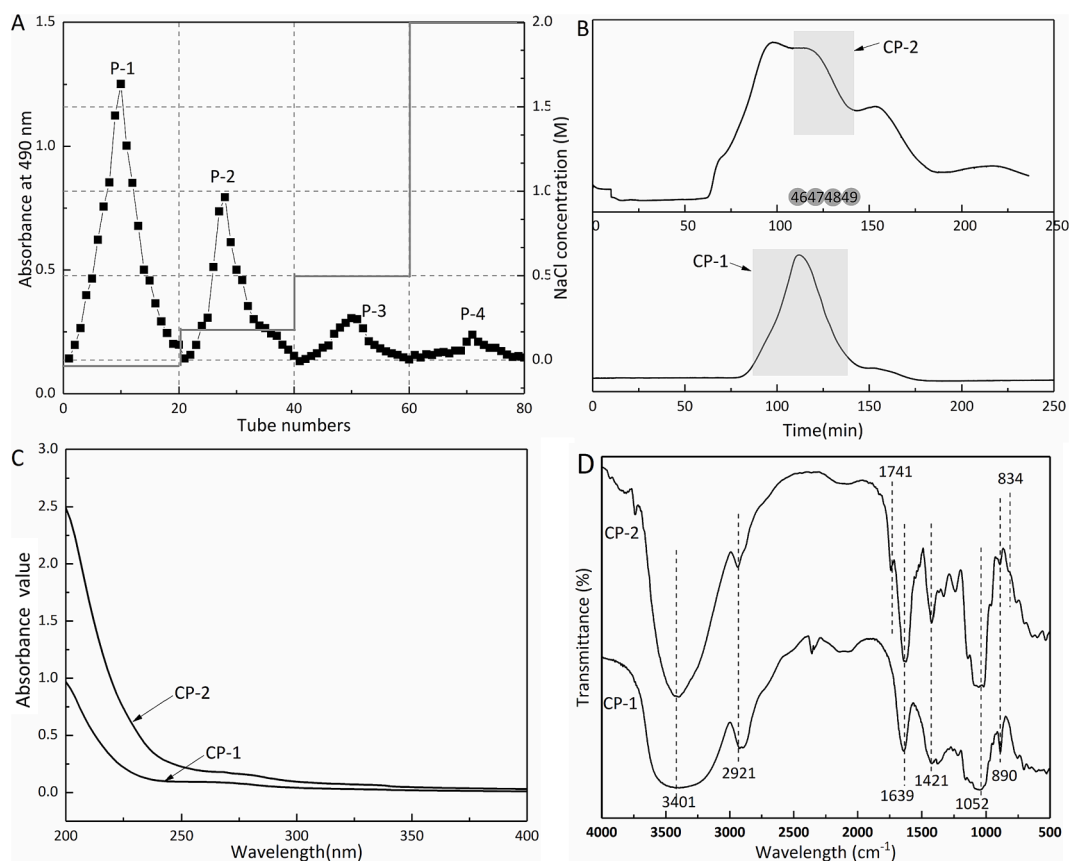

Fig. 1. (A) DEAE-52 chromatography of P-1, P-2, P-3, and P-4; (B) Profiles of CP-1 and CP-1 by Sephadex-200 chromatography; (C) UV spectra of CP-1 and CP-2; (D) FT-IR spectra of CP-1 and CP-2, respectively.

samples were loaded on a Superdex-200 column during the process. As depicted in Fig. 1B, the profile recorded for the P-1 fraction presented a single, narrow, and sharp symmetrical peak. This suggested that it was a homogeneous polysaccharide. The major elution peaks were observed and named CP-1. The profiles recorded for the P-2 fraction presented a broad peak, and the major elution peaks were observed. These peaks corresponded to the profiles recorded for the fractions recorded for the 46th, 47th, 48th, and 49th tubes. These were designated as CP-2. Finally, CP-1 and CP-2 were dialyzed and lyophilized to obtain the pure polysaccharide for structural characterization.

3.2. Molar mass distribution corresponding to CP-1 and CP-2

The HPGPC technique was used to detect the molar mass distributions of CP-1 and CP-2. The *Mw*, *Mn*, and *Mw/Mn* values of CP-1 and CP-2 were calculated, and the values were found to be 41.1 KDa, 29.4 KDa, and 1.39 for CP-1 and 15.6 KDa, 12.3 KDa, and 1.26 for CP-2. Each purified polysaccharide fraction exhibited a low polydispersity index, suggesting low polydispersity for CP-1 and CP-2 (Song et al., 2019).

3.3. Monosaccharide composition of purified polysaccharide fractions

The neutral sugar and uronic acid compositions of CP-1 and CP-2 were presented in Table 1. CP-1 was identified as a homopolysaccharide composed solely of galactose, indicating that it was a galactan. This finding aligns with the findings reported by Shiga, Peroni-Okita, Carpita, Lajolo, and Cordenunsi (2015), which revealed that chayote fruit was rich in galactan-rich pectin material. The presence of galactan contributes to the firm structure of the fruit tissue (Shiga, Peroni-Okita, Carpita, Lajolo, & Cordenunsi, 2015). Additionally, galactan exhibits excellent water-holding capacity, making chayote polysaccharides a suitable thickener that can be used in the food industry (Vieira, Pinho, Ferreira, & Delerue-Matos, 2019).

As shown in Table 1, CP-2 predominantly consisted of galacturonic acid (31.2 mol%). It also contained significant amounts of galactose (26.3 mol%), arabinose (24.9 mol%), rhamnose (7.4 mol%), glucose (6.5 mol%), glucuronic acid (1.9 mol%), mannose (1.3 mol%), and xylose (0.5 mol%). This composition suggests that CP-2 was a pectin-rich material and was similar to the cell walls of fruits (Qin, Liu, Lv, & Wang, 2020; Shiga, Peroni-Okita, Carpita, Lajolo, & Cordenunsi, 2015).

Furthermore, the higher content of galacturonic acid (31.2 mol%) and galactose (26.3 mol%) suggests that CP-2 may have a backbone composed of GalA and Gal. This result agrees with the previously reported results (Shiga et al., 2015). In a study by Shiga et al. (2015), similar monosaccharide compositions were reported for chayote fruit cell-wall water-insoluble polysaccharides. However, the galacturonic acid and galactose content was higher (20 mol% and 45 mol%, respectively) than the contents reported herein. However, the molar ratio corresponding to monosaccharide composition may differ due to significant variations in the growth region, fruit harvest period, and analytical procedures.

Table 1
Monosaccharide compositions of two cell-wall polysaccharides (CP-1 and CP-2) of chayote, respectively.

Monosaccharide composition	Molar ratios (%)	
	CP-1	CP-2
Rhamnose		7.4
Arabinose		24.9
Galactose	100	26.3
Glucose		6.5
Xylose		0.5
Mannose		1.3
Galacturonic acid		31.2
Glucuronic acid		1.9

3.4. Spectropy analysis results

The UV profiles (200–400 nm) of CP-1 and CP-2 were illustrated in Fig. 1C. There was no absorbance peak at 260 and 280 nm for CP-1 and CP-2, suggesting that nucleic acid and protein were absent in CP-1 and CP-2 samples.

Fig. 1D presents the FT-IR spectral profiles of CP-1 and CP-2. The absorption band at 3401 cm^{-1} corresponds to the stretching vibration of –OH. The presence of this band indicated the presence of intermolecular and intra-molecular hydrogen bonds. The signal at 2921 cm^{-1} corresponded to the C—H absorbance peak corresponding to the polysaccharides in the CP-1 and CP-2 samples (Wang, Liu, & Qin, 2017). The absorption peak appearing at 1741 cm^{-1} in the FT-IR profile of CP-2 was weak, indicating that uronic acid units were present in CP-2. This result was consistent with the results obtained by analyzing the monosaccharide compositions of CP-2. The absorption peak at 1639 cm^{-1} corresponded to the flexural vibration of the –OH unit (Tang et al., 2020). The peak at 1421 cm^{-1} was attributed to the stretching vibration of C—H (Zhang, Guo, Yan, Feng, & Wan, 2020). The absorption peak in the range of 1250–1000 cm^{-1} can be attributed to the absorption vibration of the C—O—C unit in the glycosidic linkages and the C–OH bending phenomenon. The presence of these peaks suggested that purified polysaccharides contained pyranose (Dranca, Vargas, & Oroian, 2020). Additionally, a weak stretching vibration peak at 890 cm^{-1} was observed in the spectral profiles recorded for CP-1 and CP-2. The appearance of this peak could be attributed to the presence of the β-glycosidic linkages in the samples. The absorption bands appearing at approximately 834 cm^{-1} in the spectral profile recorded for CP-2 indicated the presence of α-configuration in CP-2 (Wang, Liu, & Qin, 2017).

3.5. Methylation of CP-1 and CP-2

The GC–MS technique was used to study the methylation of the samples to elucidate the linkages and structural characteristics of CP-1 and CP-2. The molar ratios of various sugar residues were based on the relative retention time and the peak area recorded for PMAAs. The detailed information was summarized in Table 2. A comparison of fragmentation patterns with standard data was conducted using the GC–MS technique. The results revealed the link mode (2,3,6-Me$_3$-Gal*p* residues) to be → 4)-Gal*p*-(1 →. This result corresponded to the results obtained post FTIR and monosaccharide analysis of CP-1.

Methylation analysis revealed that CP-2 contained eleven glycosidic linkages including Ara*f*-(1→, →2)-Ara*f*-(1→, →5)-Ara*f*-(1→, Glc*p*-(1→, Gal*p*-(1→, →4)-Gal*p*-(1→, →4)-Glc*p*-(1→, →3)-Gal*p*-(1→, →6)-Gal*p*-(1→, →3,6)-Glc*p*-(1 → and → 3,6)-Gal*p*-(1 → at molar percent ratios of 10.3:7.0:7.4:4.6:6.6:16.0:12.1:10.4:4.2:5.4:16.1. These results suggested that CP-2 was a branched polysaccharide. During methylation, 1, 4-GalA was reduced to 1, 4-Gal. As summarized in Table 2, the molar ratio recorded for the 1, 4-linked Gal system was higher than that recorded for other glycosidic bonds in monosaccharides. This indicated that Gal*p*A in CP-2 may be 1, 4-linked (Chen, Zhu, Ma, Zhang, & Wu, 2019; Zhu et al., 2020). The linkages in Man*p*, Xyl*p*, and Rha*p* were not detected, possibly because of the lower Rha, Xyl, and Man contents in CP-2 and/or the degradation of the compounds during the reduction process (Zhang, 2015).

3.6. NMR analysis of CP-1 and CP-2

3.6.1. NMR analysis of CP-1

The primary structure of CP-1 was analyzed using the 1D and 2D NMR spectroscopy techniques (Fig. 2A-F).

The signals corresponding to CP-1 appeared in the range of 3.0–4.56 ppm in the ^{1}H NMR (Fig. 2A) profile and 60–106 ppm in the ^{13}C NMR (Fig. 2B) profile, which suggested that CP-1 was a typical polysaccharide. The signals appearing in the range of 4.3–5.5 ppm were attributed to the presence of β-anomers (Wang, Liu, & Qin, 2017). The

Table 2
Results of the methylation analysis of CP-1 and CP-2, respectively.

RT (min)	Methylated sugar	Mass fragments (*m/z*)	Type of linkage	Molar ratio (%)	
				CP-1	CP-2
9.342	2,3,5-Me₃-Ara*f*	43,71,87,101,117,129,145,161	Ara*f*-(1→		10.3
12.917	3,5-Me₂-Ara*f*	43,71,87,101,129,161,189	→2)-Ara*f*-(1→		7.0
14.517	2,3-Me₂-Ara*f*	43,71,87,99,101,117,129,161,189	→5)-Ara*f*-(1→		7.4
16.058	2,3,4,6-Me₄-Glc*p*	43,71,87,101,117,129,145,161,205	Glc*p*-(1→		4.6
17.358	2,3,4,6-Me₄-Gal*p*	43,71,87,101,117,129,145,161,205	Gal*p*-(1→		6.6
20.700	2,3,6-Me₃-Gal*p*	43,87,99,101,113,117,129,131,161,173,233	→4)-Gal*p*-(1→	100	16.0
21.283	2,3,6-Me₃-Glc*p*	43,87,99,101,113,117,129,131,161,173,233	→4)-Glc*p*-(1→		12.1
21.925	2,4,6-Me₃-Gal*p*	43,87,99,101,117,129,161,173,233	→3)-Gal*p*-(1→		10.4
24.267	2,3,4-Me₃-Gal*p*	43,87,99,101,117,129,161,189,233	→6)-Gal*p*-(1→		4.2
24.650	2,4-Me₂-Glc*p*	43,87,117,129,159,189,233	→3,6)-Glc*p*-(1→		5.4
29.258	2,4-Me₂-Gal*p*	43,87,117,129,159,189,233	→3,6)-Gal*p*-(1→		16.1

signals corresponding to anomeric carbons appeared at 105.8 ppm in the ^{13}C NMR profile (Fig. 2B), indicating the presence of β-configurations (103–107 ppm) (Pan et al., 2020). This result was consistent with the methylation analysis results of CP-1. The peaks at 73.21, 74.84, 79.03, 76.01, and 62.10 ppm could be attributed to the C-2, C-3, C-4, C-5, and C-6 units in β-D-Gal*p*, respectively. The chemical shifts corresponding to CP-1 were presented in Supplementary material (Table 1).

The chemical shifts corresponding to the carbon and hydrogen atoms in the sugar ring of the polysaccharide CP-1 were classified using the 2D NMR spectroscopy techniques, such as HSQC (Fig. 2C), COSY (Fig. 2D), HMBC (Fig. 2E), and NOESY (Fig. 2F). In the HSQC (Fig. 2C) profile, hetero-headed carbon signal appeared at 105.80 ppm, and the corresponding hetero-headed hydrogen signal appeared at 4.56 ppm. In the COSY (Fig. 2D) profile, the signal corresponding to H1-2 appeared at 4.56/3.60 ppm. The signal corresponding to H2-3 appeared at 3.60/3.69 ppm, the signal corresponding to H3-4 appeared at 3.69/4.08 ppm, the signal corresponding to H4-5 appeared at 4.08/3.63 ppm, and the signal corresponding to H5-6 appeared at 3.63/3.73 ppm. These results indicated that the peaks corresponding to H2, H3, H4, H5, and H6 appeared at 3.60, 3.69, 4.08, 3.63, and 3.73 ppm, respectively. The peaks corresponding to galactose C1-6 in the HSQC (Fig. 2C) profile appeared at 105.80, 73.21, 74.84, 79.03, 76.01, and 62.10 ppm. Research fronts have concluded that the signals corresponding to C-l/H-1 appeared at 105.80/4.56 ppm, and the signals corresponding to C-6/H-6 appeared at 62.10/3.73 ppm in the profile recorded for the cell-wall polysaccharides. The presence of these peaks indicates the presence of 1,4-D-galactose. Additionally, the correlation peak corresponding to H-1 and C-4 of galactose (4.56/79.03 ppm) and the cross peak corresponding to H-4 and C-1 (4.08/105.80 ppm) in the HMBC (Fig. 2E) confirmed the presence of the β-1,4-glycosidic bonds between galactose monosaccharides. Similar results were obtained by analyzing the FTIR profile and conducting methylation experiments. Furthermore, the signal corresponding to C-4 appeared downfield, indicating the influence of the C-4 unit in the glycosidic bond and the existence of → 4)-D-Gal*p*-(1→ (John, Yang, Liu, Jiang, & Yang, 2018). CP-1 was identified as galactan with no branch chains, and the probable structure has been presented in Fig. 2G.

3.6.2. NMR analysis of CP-2

The structural characteristics of CP-2 were identified by analyzing the NMR spectral profiles, as shown in Fig. 3A-F. The ^{1}H NMR signals were primarily distributed in the range of 3.0–5.5 ppm. The signals corresponding to the primary anomeric protons appeared at 5.17, 5.02, 5.04, 4.37, 4.56, 4.42, 4.40, and 4.46 ppm. As depicted in Fig. 3A, the anomeric signals at 5.17 and 5.02 ppm represented α-configuration, and the signals in the range of 4.4–5.0 ppm region represented the β-configuration (Song et al., 2019). The ^{13}C NMR peaks corresponding to CP-2 appeared in the range of 60–120 ppm (Fig. 3B). Analysis of the spectral profiles reveals the typical characteristic of polysaccharides (Song et al., 2019). The signals corresponding to anomeric carbon appeared in the region of 100–110 ppm, and this indicated the presence

of α- and β-glycosidic bonds. The results were consistent with the ^{1}H NMR analysis results. The eight signals at 110.62, 108.60, 101.87, 104.90, 105.74, 104.69, 104.48, and 103.84 ppm were assigned to A, B, C, D, E, F, G, and H residues, respectively (Fig. 3B).

The chemical shift data corresponding to CP-2 were presented in Supplementary material file (Supplementary Table 1). The results were based on the information obtained by analyzing the 1D NMR and HSQC (Fig. 3C), COSY (Fig. 3D), HMBC (Fig. 3E), and NOESY (Fig. 3F) spectral profiles. The comparison was made based on previously reported data (Song et al., 2019; Yao, Yao, Du, Wang, & Ding, 2018). The NMR profiles corresponding to CP-2 presented peaks corresponding to galacturonic acids, galactose, and arabinose. This indicated that galacturonic acids, galactose, and arabinose were the major constituents of CP-2. Prominent signals were not recorded for rhamnose, xylose, mannose, and glucuronic acid, and this could be potentially attributed to the low content of these monosaccharides. This result was consistent with the monosaccharide composition and methylation results. Alba et al. (2020) reported the absence of signals corresponding to rhamnose in the NMR profiles. The absence of these peaks was attributed to the low content of rhamnose, and the results reflected the results presented herein.

The signal corresponding to the anomeric carbon in residue A appeared at 110.62 ppm. A cross peak for A H1-C1 (5.17/110.62 ppm) appeared in the HSQC profile (Fig. 3C), and the signal corresponding to the anomeric proton appeared at 5.17 ppm. This revealed the α-configuration (Li et al., 2018) of the samples. Correlations corresponding to A H1/H2, A H2/H3, A H3/H4, A H4/H5, and A H5/H5b were recorded in the COSY profile (Fig. 3D). The signals for A H2–A H5b appeared at 4.13, 3.87, 4.06, 3.76, and 3.64 ppm. The HSQC (Fig. 3C) correlations were studied: A H1-C1, A H2-*C*2, A H3-C3, A H4-C4, A H5-C5, A H5b-C6. The chemical shifts of the peaks corresponding to A *C*2–A C5 were 82.62, 77.97, 85.22, and 62.64 ppm, respectively. The results were compared with previously reported results (Guo, Zhang, Wang, Li, & Ding, 2020; Yang et al., 2018), and the data indicated that residue A presented an α-L-Ara*f*-(1 → structure.

The cross peak corresponding to B H1-C1 (5.02/108.60 ppm) in the HSQC (Fig. 3C) profile corresponded to the anomeric proton and carbon in residue B. The cross peaks corresponding to B H1/H2, B H2/H3, B H3/H4, B H4/H5, and B H5/H5b in the COSY (Fig. 3D) profile indicated that the peaks corresponding to B H2–B H5b appeared at 4.07, 3.96, 4.16, 3.81, and 3.72 ppm. In addition, the corresponding carbon signals appeared in the HSQC (Fig. 3C) profile. The peaks appeared at 82.52, 78.12, 83.60, and 67.60 ppm. Based on literature data (Guo, Zhang, Wang, Li, & Ding, 2020) and NMR analysis, residue B was identified as → 5)-α-L-Ara*f*-(1 →.

The cross peaks (C H1/H2, C H2/H3, C H3/H4, and C H4/H5) corresponding to residue C appeared at 5.04/3.66, 3.66/3.94, 3.94/4.52, and 4.52/4.72 ppm in the COSY (Fig. 3D) profile, and these peaks were assigned to the C H2–C H5 units. The anomeric carbon signal corresponding to residue C appeared at 101.87 ppm. Subsequently, the signals corresponding to C C1–C6 were assigned based on the cross peaks (C H1-C1, C H2-*C*2, C H3-C3, C H4-C4, and C H5-C5) in the HSQC profile
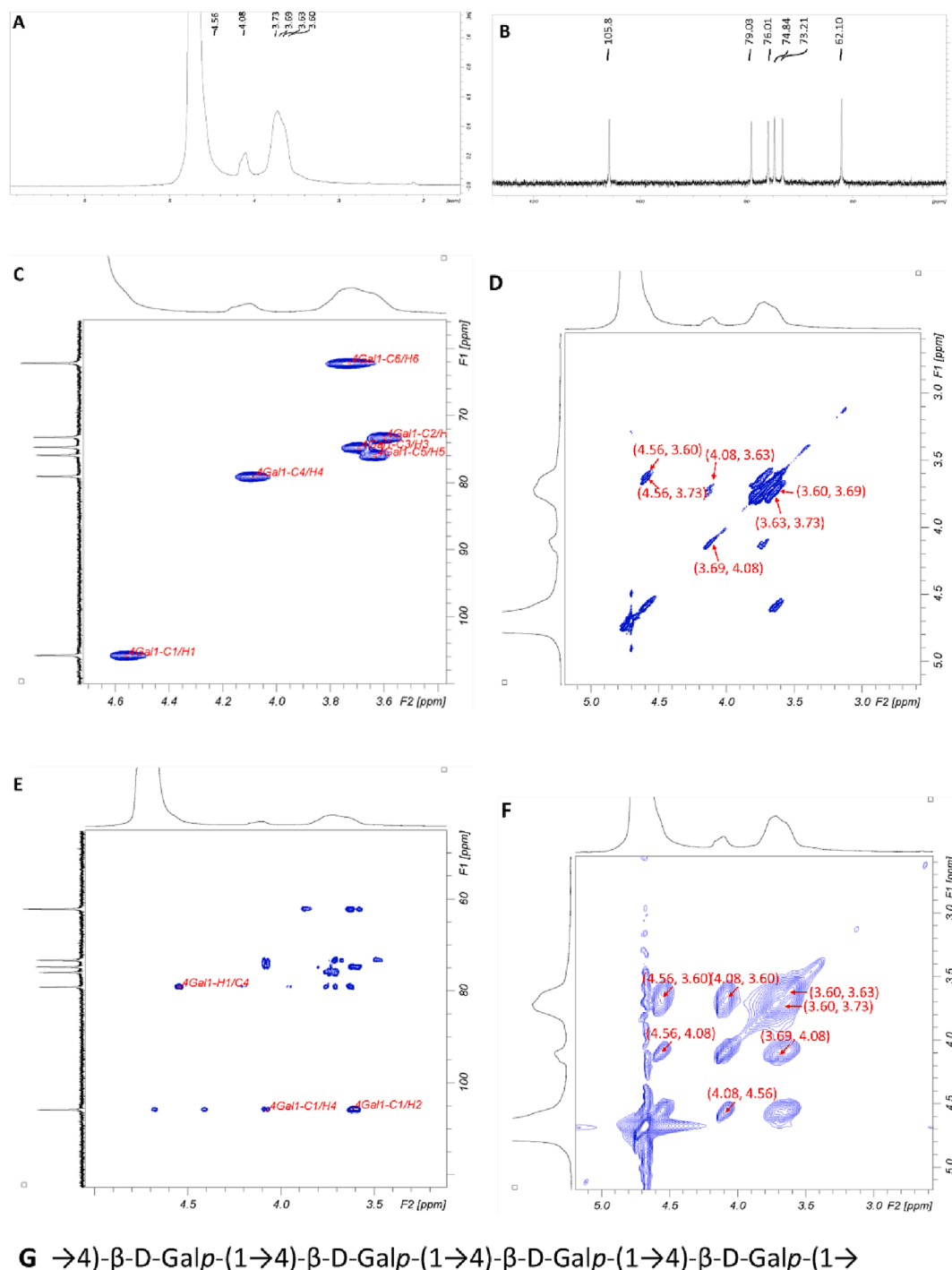
Fig. 2. (A) ^{1}H NMR spectrum of CP-1; (B) ^{13}C NMR spectrum of CP-1; (C) HSQC spectrum of CP-1; (D) ^{1}H–^{1}H COSY spectrum of CP-1; (E) HMBC spectrum of CP-1; (F) NOESY spectrum of CP-1; (G) Speculated chemical structure of CP-1.

(Fig. 3C). The presence of a peak at 176.24 ppm indicated the presence of an esterified carboxyl unit in C C6. Cross peaks corresponding to 3.74/54.23 ppm were assigned to CH$_3$ units, while the peak corresponding to CH$_3$CO appeared at 1.86/21.20 ppm in the HSQC profile (Fig. 3C). The results confirmed the presence of GalpA (Liu et al., 2018). The results revealed that residue C presented the → 4)-α-D-GalpA-(1 → structure. The conclusion was made based on methylation data, NMR data, and analysis of literature reports (Colodel, Bagatin, Tavares, & Petkowicz, 2017).

The peaks at 4.37/104.90 ppm (D H1/C1) in the HSQC (Fig. 3C) profile corresponded to the anomeric signals of residue D. The peaks

corresponding to a primary alcohol (–CH$_2$OH) appeared at 3.83 and 3.61/69.00 ppm. These were attributed to D H6b, D H5b-C5 of residue D. The downfield shift of the D C6 unit (69.00 ppm) suggested that it contributed to the glycosidic bond of → 6)-β-D-Galp-(1→ (Liu et al., 2018).

The peak at 105.74 ppm was attributed to the anomeric carbon of residue E. The cross peak appeared at 4.56/105.74 ppm (E H1-C1) in the HSQC profile (Fig. 3C), and the peak corresponding to the anomeric proton appeared at 4.56 ppm. The cross peak (4.56/105.74 ppm) in the HSQC profile (Fig. 3C) was attributed to anomeric proton and carbon unit in D-Galp. The presence of these peaks indicated the presence of a
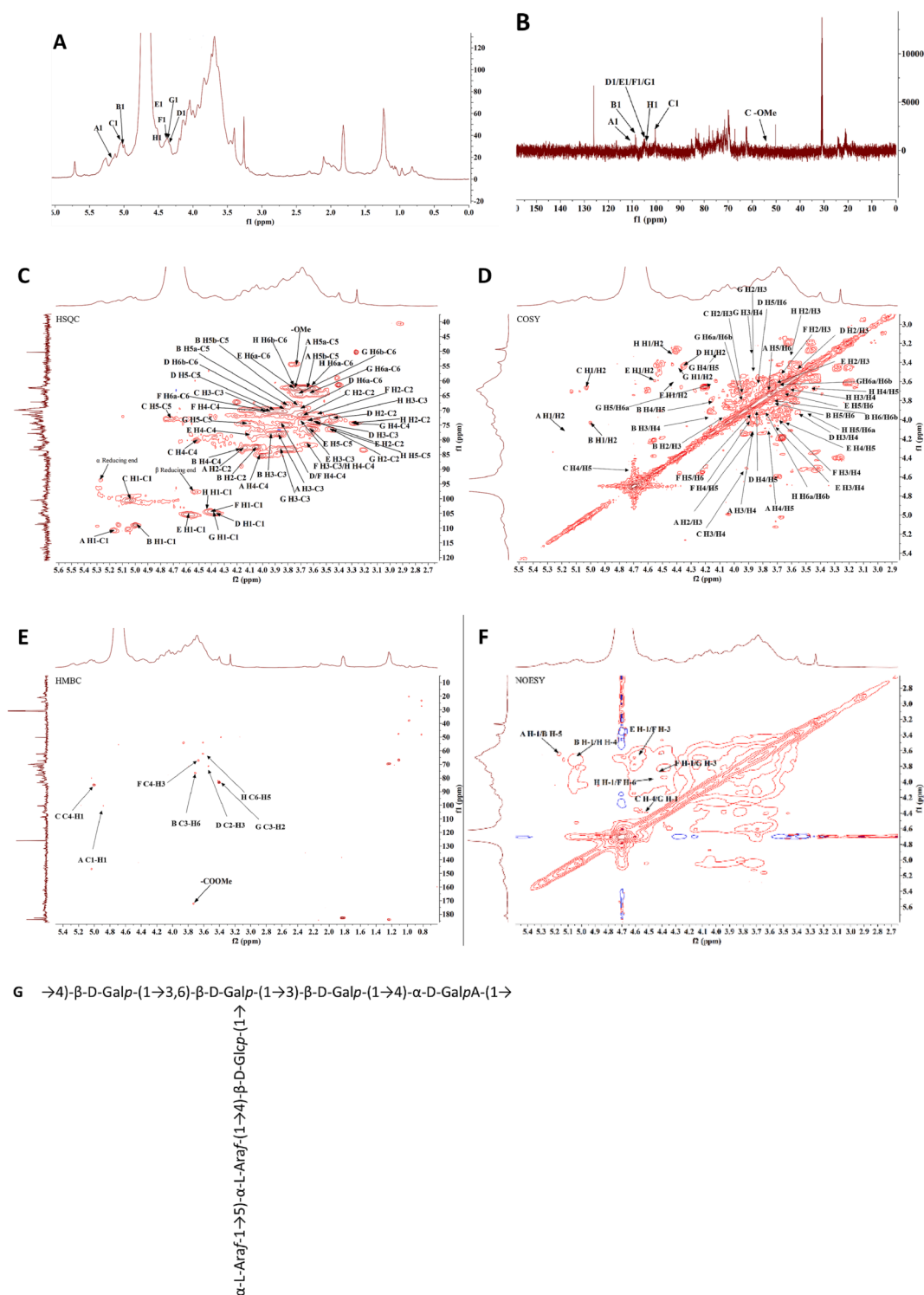
Fig. 3. (A) ¹H NMR spectrum of CP-2; (B) ¹³C NMR spectrum of CP-2; (C) HSQC spectrum of CP-2; (D) ¹H–¹H COSY spectrum of CP-2; (E) HMBC spectrum of CP-2; (F) NOESY spectrum of CP-2; (G) Speculated chemical structure of CP-2.

β-type configuration (Liu et al., 2018). The signals corresponding to E H2–E H6 were assigned based on the cross peaks corresponding to E H1/ H2, E H2/H3, E H3/H4, E H4/H5, and E H5/H6 in the COSY profile (Fig. 3D). The peaks appeared at 3.60, 3.70, 4.08, 3.65, and 3.74 ppm. Moreover, the chemical shifts of the peaks corresponding to E C-1–C-6 were identified from the HSQC profile (Fig. 3C). Residue E was identified as → 4)-β-D-Galp-(1 → based on the NMR analysis and data presented in literature reports (Yue, Xu, Bian, Guo, Fang, & Wu, 2020;

Zhang, Chen, & Ding, 2019).

The signals corresponding to the anomeric protons in residues F and G appeared at 4.42 and 4.40 ppm, respectively, suggesting that they presented β-configuration. Peaks corresponding to F H1-C1 and G H1-C1 appeared at 4.42/104.69 and 4.40/104.48 ppm, respectively. Analysis of the HSQC profile (Fig. 3C) indicated that the F residue presented the → 3,6)-β-D-Galp-(1 → structure. Similarly, the cross-peak at 3.88/82.70 ppm (G H3-C3) in the profile recorded for residue G demonstrated that G

C3 was substituted. Hence, it was inferred that residue G presented the → 3)-β-D-Gal*p*-(1 → structure (Li et al., 2018; Liu et al., 2018).

As for residues H H C1 and H H1, chemical shifts appeared at 103.84 and 4.46 ppm, respectively. The H C1 peak at 103.84 ppm indicated a β-configuration. COSY correlations (H H1/H2, H H2/H3, and H H3/H4) (Fig. 3D) indicated that the signals corresponding to H H2–H H4 appeared at 3.30, 3.63, and 3.64 ppm. The peaks corresponding to H H5, H H6a, and H H6b appeared at 3.47, 3.95, and 3.79 ppm, respectively. The inference was made based on NOESY data (Fig. 3F). Besides, the signals corresponding to H *C*2–H C6 were extracted based on the cross peaks (H H1-C1, H H2-*C*2, H H3-C3, H H4-C4, H H5-C5, and H H6a-C6) in the HSQC profile (Fig. 3C). According to the data in the reference, residue H was identified as → 4)-β-D-Glc*p*-(1 →.

The glycosidic linkage sequences corresponding to the backbone and side chains were identified by analyzing the NOESY profile (Fig. 3F) and correlative references (Chen, Zhu, Ma, Zhang, & Wu, 2019; Zhang, Guo, Yan, Feng, & Wan, 2020). The cross peak E H-1/F H-3 (4.56/3.68 ppm) presented the relevance to H-1 of → 4)-β-D-Gal*p*-(1 → and H-3 of neighbouring → 3,6)-β-D-Gal*p*-(1→, presence sequences of → 4)-β-D-Gal*p*-(1 → 3,6)-β-D-Gal*p*-(1 →. The cross peak F H-1/G H-3 (4.42/3.88 ppm) presented the correlate of H-1 of → 3,6)-β-D-Gal*p*-(1 → and H-3 of → 3)-β-D-Gal*p*-(1 → presence sequences of → 3,6)-β-D-Gal*p*-(1 → 3)-β-D-Gal*p*-(1 →. The cross peak G H-1/C H-4 (4.40/4.52 ppm) presented the correlate of H-1 of → 3)-β-D-Gal*p*-(1 → and H-4 of → 4)-α-D-GalpA-(1→, presence sequences of → 3)-β-D-Gal*p*-(1 → 4)-α-D-GalpA-(1 →. The cross peak H H-1/F H-6 (4.46/3.96 ppm) presented the correlation between H-1 of → 4)-β-D-Glc*p*-(1 → and H-6 of → 3,6)-β-D-Gal*p*-(1→, presence sequences of → 4)-β-D-Glc*p*-(1 → 3,6)-β-D-Gal*p*-(1→ (Chen, Zhu, Ma, Zhang, & Wu, 2019). The side chain was composed of α-L-Ara*f*-(1→, →5)-α-L-Ara*f*-(1→, and → 4)-β-D-Glc*p*-(1 →. The cross peak A H-1/B H-5 (5.17/3.81 ppm) presented the correlation between H-1 of → 5)-α-L-Ara*f*-(1 → and H-5 of → 5)-α-L-Ara*f*-(1→, presence sequences of α-L-Ara*f*-(1 → 5)-α-L-Ara*f*-(1 →. The cross peak B H-1/H H-4 (5.02/3.64 ppm) presented the correlation between H-1 of → 5)-α-L-Ara*f*-(1 → and H-4 of → 4)-β-D-Glc*p*-(1→, presence sequences of → 5)-α-L-Ara*f*-(1 → 4)-β-D-Glc*p*-(1→ (Chen, Zhu, Ma, Zhang, & Wu, 2019).

Methylation, monosaccharide composition, and FTIR data revealed that the backbone of CP-2 consisted of → 4)-β-D-Gal*p*-(1 → 3,6)-β-D-Gal*p*-(1 → 3)-β-D-Gal*p*-(1 → 4)-α-D-GalpA-(1 →. The branched chain was α-L-Ara*f*-(1 → 5)-α-L-Ara*f*-(1 → 4)-β-D-Glc*p*-(1→, and it was attached to the backbone chain O-6 in → 3,6)-β-D-Gal*p*-(1 →. In conclusion, the probable structure of CP-2 was proposed, and it has been depicted in Fig. 3G. The chemical structure of pectin polysaccharide isolated from the petals of *Saussurea laniceps* was similar to the chemical structure of CP-2. (Chen, Zhu, Ma, Zhang, & Wu, 2019).

3.7. Physicochemical properties

The surface morphology of CP-1 and CP-2 fractions magnified 200 times using the SEM technique were presented in Fig. 4A and B, respectively. CP-1 presented an irregular reticulation and contains pores of various sizes. The excellent water solubility of CP-1 can be attributed to the presence of these pores. The network morphology of polysaccharides presented in Senegrain seeds (Ktari, Bkhairia, Nasri, & Ben Salah, 2020) and Chinese wild fruits (*Passiflora foetida*) (Song et al., 2019) has been previously reported. Unlike CP-1, CP-2 presents a sheet-like compact amorphous morphology with a relatively smooth, well-regulated, and homogeneous surface which resembles the morphology of polysaccharides extracted from *Cordyceps militaris* (Wu et al., 2020) and *Hypsizygus marmoreus* (Song, Teng, & Zhu, 2020).

The nanostructure of polysaccharides (CP-1 and CP-2) was analyzed using the AFM technique, and the 2D and 3D AFM images were presented in Fig. 4C-F. Analysis of the 2D images revealed the presence of bright regions. The presence of these regions can be attributed to the aggregation of polymers during sample preparation and the strong intermolecular interaction between polysaccharide molecules (Qin, Liu,

Lv, & Wang, 2020). The extent of molecular aggregation observed for CP-1 with high *Mw* was higher than that observed in CP-2. As depicted in Fig. 4C and E, the height of CP-1 was approximately 3.5 nm, and it presented flame aggregation properties, which might be related to the linear structure of CP-1 (Qu, Gao, Zhao, Wang, & Yi, 2019). The height properties of CP-1 could be attributed to the intermolecular winding structures, which presented a highly stable helical structure (Hong & Ying, 2019). The height of CP-2 (Fig. 4D and F) was approximately 1.3 nm, and the sugar chain presented flame-like aggregation properties to a certain extent. This might be attributed to the molecules being connected via intermolecular hydrogen bonds (Hong & Ying, 2019). This aggregation may be related to the branching structure of CP-2 (Wang, Liu, & Qin, 2017). The physicochemical properties of CP-1 and CP-2 were studied using the SEM and AFM techniques, and the results were consistent.

The XRD technique was used to analyze the degree of crystallinity of CP-1 and CP-2, and the results were presented in Fig. 4G and H, respectively. As depicted in Fig. 4G, two primary reflections appeared at 13.78° and 23.52°, implying that CP-1 presented two primary crystalline phases (Gao et al., 2020). The XRD patterns recorded for CP-2 (Fig. 4H) revealed the presence of a broad peak, and this confirmed the non-crystal structure of CP-2 (Zhang, Kong, Hao, Zhang, & Zhu, 2020). Therefore, it was inferred that CP-1 was semi-crystalline while CP-2 was amorphous (Liu, Li, Fan, Zhang, & Zhong, 2019).

4. Discussion

Chayote is a widely popular herbaceous perennial climbing plant known for its nutrient-rich flesh, low-calorie content, and low-fat content (Vieira, Pinho, Ferreira, & Delerue-Matos, 2019). As essential components of plant foods, polysaccharides have also garnered significant attention from researchers. In the current study, the neutral polysaccharide fraction (CP-1) was eluted using deionized water, while the anionic polysaccharide fraction (CP-2) was eluted with NaCl (0.2 mol·L⁻¹). CP-1 was identified as a linear galactan. Galactan is typically found in unripe fruits such as apples and papayas (John, Yang, Liu, Jiang, & Yang, 2018) and contributes to the structural integrity of fruit tissues. Chayote is typically consumed when it is still unripe, as the fruit becomes hard and unsuitable for consumption after ripening (Shiga, Peroni-Okita, Carpita, Lajolo, & Cordenunsi, 2015). In this study, 200 g of chayote was harvested before ripening, making galactan identification reasonable. Previous research has also reported that chayote fruit is rich in dietary fibers, particularly linear galactan, and arabinans (Modgil, Modgil, & Kumar, 2004). Furthermore, linear galactan and arabinans exhibit higher water-holding capacity compared to branched arabinans (Shiga, Peroni-Okita, Carpita, Lajolo, & Cordenunsi, 2015). The abundance of galactan suggests that chayote cell-wall polysaccharides could be utilized as thickeners in food emulsions or baked goods. Interestingly, John et al. (2018) compared the water-soluble polysaccharides in papaya at different stages of ripeness and found that galactan was present in all-green papaya but not in ripe papaya (John, Yang, Liu, Jiang, & Yang, 2018). Additionally, Zhang, Chen, and Ding (2019) obtained 1,4-β-galactan from *Dioscorea opposita*.

Another polysaccharide purified from chayote, CP-2, was identified as a heteropolysaccharide. The variation in monosaccharide composition compared to previous research (Shiga, Peroni-Okita, Carpita, Lajolo, & Cordenunsi, 2015) could be attributed to differences in the growing environments and harvesting periods. The extraction, purification techniques, and detection methods employed can also influence the polysaccharide components. Chen et al. (2019) reported similar monosaccharide compositions in the petal pectin polysaccharide obtained from *Saussurea laniceps*. It was observed that galacturonic acid, galactose, arabinose, rhamnose, glucose, mannose, and xylose were present in specific molar ratios. CP-2 exhibited a branched structure with side chains of *t*-Ara*f* ramification (arabinoglucan). A similar side structure (*t*-Ara*f*) was found in the polysaccharide SMP-0b purified from
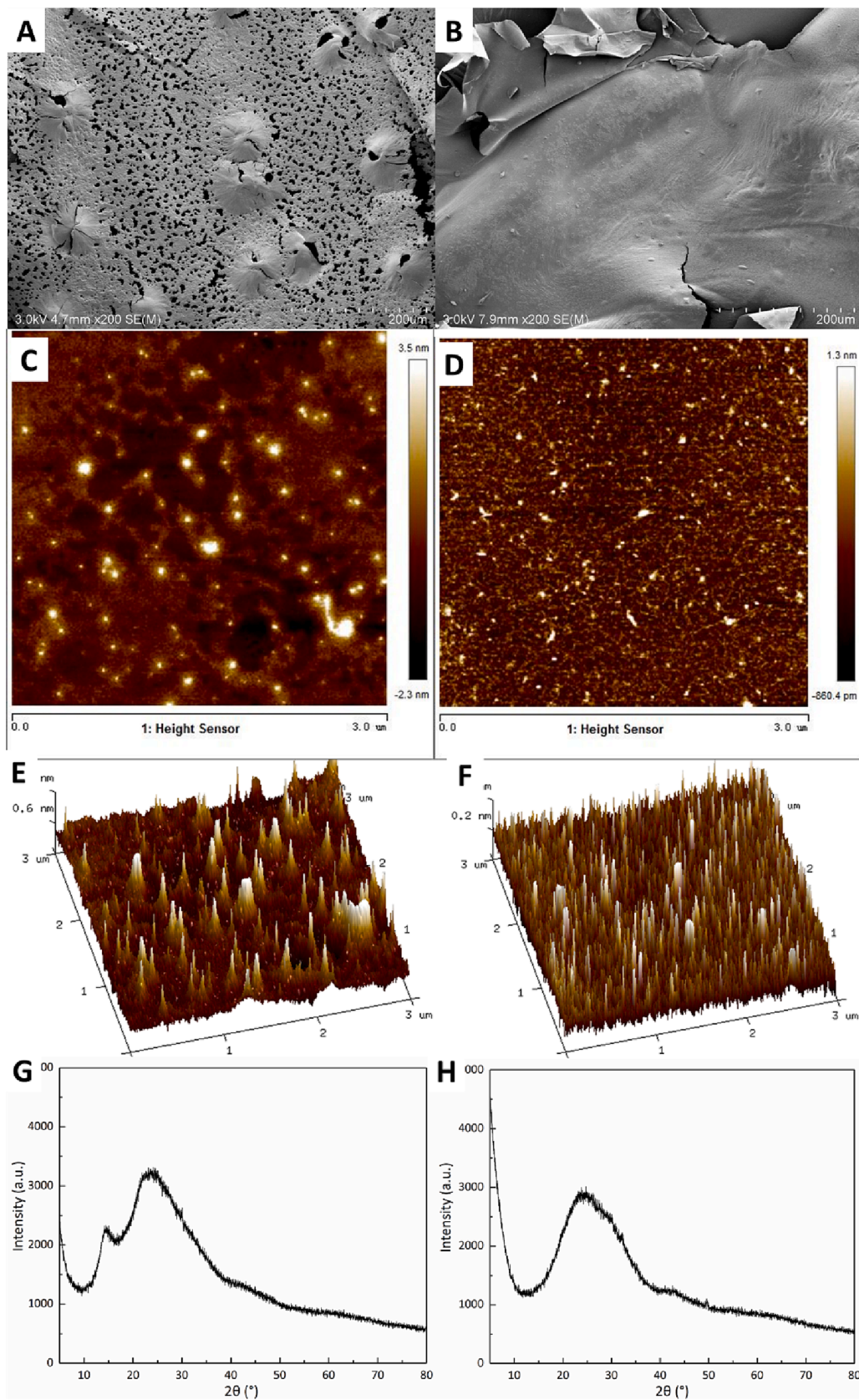
Fig. 4. (A) SEM image (200 ×) of CP-1; (B) SEM image (200 ×) of CP-2; (C) 2D AFM image of CP-1; (D) 2D AFM imagesof CP-2; (E) 3D AFM image of CP-1; (F) 3D AFM image of CP-2; (G) XRD curve of CP-1; (H) XRD curve of CP-2.

Solanum muricatum (Yue, Xu, Bian, Guo, Fang, & Wu, 2020).

The molecular weight of CP-1 and CP-2 purified from chayote was relatively low, with values of 41.1 KDa and 15.6 KDa, respectively, which were lower than those of the polysaccharides isolated from Senegrain seeds (47.42 KDa) (Ktari, Bkhairia, Nasri, & Ben Salah, 2020) and *Tetrastigma hemsleyanum* Diels et Gilg (77.9 KDa) (Ru et al., 2019). The micromorphology results indicated that CP-1 presented a network morphology, while CP-2 presented a lamellar structure. These two morphologies are commonly observed in plant polysaccharides. Further research on the bioactivities and structure–activity relationships of these two cell-wall polysaccharide fractions purified from chayote is warranted to explore their potential applications.

5. Conclusions

The two cell-wall polysaccharides isolated from chayote, CP-1 and CP-2, have been characterized. CP-1 was a linear homogenous galactan with a network structure, while CP-2 was an anionic heteropolysaccharide composed of various monosaccharides, including galacturonic acid, galactose, arabinose, rhamnose, glucose, glucuronic acid, mannose, and xylose. CP-2 also presents a side chain of *t*-Araf and a sheet-like compact amorphous morphology. The results from chemical and physical structural analysis highlight the favorable application properties of CP-1 and CP-2, particularly in the food industry. These findings contribute to the utilization of chayote and its by-products and offer the potential for developing functional products derived from chayote. Furthermore, the structural data obtained for these polysaccharides can serve as valuable information for future structure–activity relationship studies.

CRediT authorship contribution statement

Jingxuan Ke: Resources, Methodology, Data curation, Writing – original draft, Funding acquisition. **Yuhao Zhang:** Investigation, Funding acquisition. **Xin Wang:** Writing – review & editing. **Jing Sun:** Conceptualization. **Siqi Wang:** Investigation. **Yanli Ma:** Writing – review & editing. **Qing Guo:** Visualization. **Zhiqing Zhang:** Funding acquisition, Supervision, Writing – review & editing.

Declaration of Competing Interest

The authors declare that they have no known competing financial interests or personal relationships that could have appeared to influence the work reported in this paper.

Data availability

Data will be made available on request.

Acknowledgements

Appendix A. Supplementary data

Supplementary data to this article can be found online at https://doi.org/10.1016/j.fochx.2023.100797.

References

Alba, K., Offiah, V., Laws, A. P., Falade, K. O., & Kontogiorgos, V. (2020). Baobab polysaccharides from fruits and leaves. *Food Hydrocolloids, 106*, Article 105874.

Aung, L. H., Ball, B., & Kushad, M. (1990). Developmental and Nutritional Aspects of Chayote (*Sechium edule*, Cucurbitaceae). *Economic Botany, 44*(2), 157–164.

Castro-Alves, V. C., & do Nascimento, J. R. O. (2016). Polysaccharides from raw and cooked chayote modulate macrophage function. *Food Research International, 81*, 171–179.

Chen, W., Zhu, X., Ma, J., Zhang, M., & Wu, H. (2019). Structural Elucidation of a Novel Pectin-Polysaccharide from the Petal of *Saussurea laniceps* and the Mechanism of its Anti-HBV Activity. *Carbohydrate Polymers, 223*, Article 115077.

Colodel, C., Bagatin, R. M.d. G., Tavares, T. M., & Petkowicz, C. L.d. O. (2017). Cell wall polysaccharides from pulp and peel of cubiu: A pectin-rich fruit. *Carbohydrate Polymers, 174*, 226–234.

Dranca, F., Vargas, M., & Oroian, M. (2020). Physicochemical properties of pectin from *Malus domestica* 'Fălticeni' apple pomace as affected by non-conventional extraction techniques. *Food Hydrocolloids, 100*, Article 105383.

Fernandes, P. A. R., & Coimbra, M. A. (2023). The antioxidant activity of polysaccharides: A structure-function relationship overview. *Carbohydrate Polymers, 314*, Article 120965.

Gao, X., Qu, H., Shan, S., Song, C., Baranenko, D., Li, Y., & Lu, W. (2020). A novel polysaccharide isolated from *Ulva Pertusa*: Structure and physicochemical property. *Carbohydrate Polymers, 233*, Article 115849.

Guo, C., Zhang, S., Wang, Y., Li, M., & Ding, K. (2020). Isolation and structure characterization of a polysaccharide from *Crataegus pinnatifida* and its bioactivity on gut microbiota. *International Journal of Biological Macromolecules, 154*, 82–91.

Hong, Y., & Ying, T. (2019). Isolation, molecular characterization and antioxidant activity of a water-soluble polysaccharide extracted from the fruiting body of *Termitornyces albuminosus* (Berk.) Heim. *International Journal of Biological Macromolecules, 122*, 115–126.

Ji, X., Guo, J., Gao, T., Zhang, T., Liu, Y., & Yan, Y. (2023). Review on mechanisms and structure-activity relationship of hypoglycemic effects of polysaccharides from natural resources. *Food Science and Human Wellness, 12*, 1969–1980.

John, A., Yang, J., Liu, J., Jiang, Y., & Yang, B. (2018). The structure changes of water-soluble polysaccharides in papaya during ripening. *International Journal of Biological Macromolecules, 115*, 152–156.

Ke, J., Jiang, G., Shen, G., Wu, H., Liu, Y., & Zhang, Z. (2020). Optimization, characterization and rheological behavior study of pectin extracted from chayote (*Sechium edule*) using ultrasound assisted method. *International Journal of Biological Macromolecules, 147*, 688–698.

Ktari, N., Bkhairia, I., Nasri, M., & Ben Salah, R. (2020). Structure and biological activities of polysaccharide purified from Senegrain seed. *International Journal of Biological Macromolecules, 144*, 190–197.

Li, B., Zhang, N., Wang, D. X., Jiao, L., Tan, T., Wang, J., … Jiang, D. C. (2018). Structural analysis and antioxidant activities of neutral polysaccharide isolated from *Epimedium koreanum* Nakai. *Carbohydrate Polymers, 196*, 246–253.

Liu, D., Li, Z., Fan, Z., Zhang, X., & Zhong, G. (2019). Effect of soybean soluble polysaccharide on the pasting, gels, and rheological properties of kudzu and lotus starches. *Food Hydrocolloids, 89*, 443–452.

Liu, J., Zhao, Y., Wu, Q., John, A., Jiang, Y., Yang, J., … Yang, B. (2018). Structure characterisation of polysaccharides in vegetable "okra" and evaluation of hypoglycemic activity. *Food Chemistry, 242*, 211–216.

Modgil, M., Modgil, R., & Kumar, R. (2004). Carbohydrate and Mineral Content of Chayote (*Sechium edule*) and Bottle Gourd (*Lagenaria Siceraria*). *Journal of Human Ecology, 15*(2), 157–159.

Pan, L. C., Zhu, Y. M., Zhu, Z. Y., Xue, W., Liu, C. Y., Sun, H. Q., & Yue, Y. (2020). Chemical structure and effects of antioxidation and against alpha-glucosidase of natural polysaccharide from *Glycyrrhiza inflata* Batalin. *International Journal of Biological Macromolecules, 155*, 560–571.

Qin, Z., Liu, H. M., Lv, T. T., & Wang, X. D. (2020). Structure, rheological, thermal and antioxidant properties of cell wall polysaccharides from Chinese quince fruits. *International Journal of Biological Macromolecules, 147*, 1146–1155.

Qu, H., Gao, X., Zhao, H. T., Wang, Z. Y., & Yi, J. J. (2019). Structural characterization and in vitro hepatoprotective activity of polysaccharide from pine nut (*Pinus koraiensis* Sieb. et Zucc.). *Carbohydrate Polymers, 223*, Article 115056.

Ru, Y., Chen, X., Wang, J., Guo, L., Lin, Z., Peng, X., … Wong, W. L. (2019). Structural characterization, hypoglycemic effects and mechanism of a novel polysaccharide from *Tetrastigma hemsleyanum* Diels et Gilg. *International Journal of Biological Macromolecules, 123*, 775–783.

Shiga, T. M., Peroni-Okita, F. H., Carpita, N. C., Lajolo, F. M., & Cordenunsi, B. R. (2015). Polysaccharide composition of raw and cooked chayote (*Sechium edule* Sw.) fruits and tuberous roots. *Carbohydrate Polymers, 130*, 155–165.

Song, Q., Teng, A.-G., & Zhu, Z. (2020). Chemical structure and inhibition on α-glucosidase of a novel polysaccharide from *Hypsizygus marmoreus*. *Journal of Molecular Structure, 1211*, Article 128110.

Song, Y., Zhu, M., Hao, H., Deng, J., Li, M., Sun, Y., … Huang, R. (2019). Structure characterization of a novel polysaccharide from Chinese wild fruits (*Passiflora foetida*) and its immune-enhancing activity. *International Journal of Biological Macromolecules, 136*, 324–331.

Tang, W., Liu, C., Liu, J., Hu, L., Huang, Y., Yuan, L., … Nie, S. (2020). Purification of polysaccharide from *Lentinus edodes* water extract by membrane separation and its chemical composition and structure characterization. *Food Hydrocolloids, 105*, Article 105851.

Vieira, E. F., Pinho, O., Ferreira, I., & Delerue-Matos, C. (2019). Chayote (*Sechium edule*): A review of nutritional composition, bioactivities and potential applications. *Food Chemistry, 275*, 557–568.

Wang, m., Hu, W. J., Wang, Q. H., Yang, B. Y., Kuang, H. X. (2023). Extraction, purification, structural characteristics, biological activities, and application of the polysaccharides from Nelumbo nucifera Gaertn. (lotus): A review. *International Journal of Biological Macromolecules 226,* 562-579.

Wang, L., Liu, H. M., & Qin, G. Y. (2017). Structure characterization and antioxidant activity of polysaccharides from Chinese quince seed meal. *Food Chemistry, 234*, 314–322.

Wu, L., Sun, H., Hao, Y., Zheng, X., Song, Q., Dai, S., & Zhu, Z. (2020). Chemical structure and inhibition on alpha-glucosidase of the polysaccharides from *Cordyceps militaris* with different developmental stages. *International Journal of Biological Macromolecules, 148*, 722–736.

Yang, J. S., Mu, T. H., & Ma, M. M. (2018). Extraction, structure, and emulsifying properties of pectin from potato pulp. *Food Chemistry, 244*, 197–205.

Yang, J., Wen, L., Zhao, Y., Jiang, Y., Tian, M., Liu, H., … Yang, B. (2018). Structure identification of an arabinogalacturonan in *Citrus reticulata* Blanco 'Chachiensis' peel. *Food Hydrocolloids, 84*, 481–488.

Yao, Y., Yao, J., Du, Z., Wang, P., & Ding, K. (2018). Structural elucidation and immune-enhancing activity of an arabinogalactan from flowers of *Carthamus tinctorius* L. *Carbohydrate Polymers, 202*, 134–142.

Yue, H., Xu, Q., Bian, G., Guo, Q., Fang, Z., & Wu, W. (2020). Structure characterization and immunomodulatory activity of a new neutral polysaccharide SMP-0b from *Solanum muricatum*. *International Journal of Biological Macromolecules, 155*, 853–860.

Zhang, C. Q., Chen, X., & Ding, K. (2019). Structural characterization of a galactan from *Dioscorea opposita* Thunb. and its bioactivity on selected Bacteroides strains from human gut microbiota. *Carbohydrate Polymers, 218*, 299–306.

Zhang, X., Kong, X., Hao, Y., Zhang, X., & Zhu, Z. (2020). Chemical structure and inhibition on alpha-glucosidase of polysaccharide with alkaline-extracted from glycyrrhiza inflata residue. *International Journal of Biological Macromolecules, 147*, 1125–1135.

Zhang, Z., Guo, L., Yan, A., Feng, L., & Wan, Y. (2020). Fractionation, structure and conformation characterization of polysaccharides from *Anoectochilus roxburghii*. *Carbohydrate Polymers, 231*, Article 115688.

Zhao, X., Moates, G. K., Wellner, N., Collins, S. R., Coleman, M. J., & Waldron, K. W. (2014). Chemical characterisation and analysis of the cell wall polysaccharides of duckweed (*Lemna minor*). *Carbohydrate Polymers, 111*, 410–418.

Zhu, M., Huang, R., Wen, P., Song, Y., He, B., Tan, J., … Wang, H. (2020). Structural characterization and immunological activity of pectin polysaccharide from kiwano (*Cucumis metuliferus*) peels. *Carbohydrate Polymers, 254*, Article 117371.

Zhang, H. (2015). *Structure and Conformational Properties of Polysaccharides from Ganoderma atrum*. Nanchang University.